Geophys. J. R. astr. Soc. (1986) **84**, 455–473

Hugoniot equation of state of anorthite glass and lunar anorthosite

Mark B. Boslough*, Sally M. Rigden and Thomas J. Ahrens *Seismological Laboratory, California Institute of Technology, Pasadena, California 91125, USA*

Accepted 1985 March 1. Received 1985 February 25; in original form 1984 March 4

Summary. Twenty-one Hugoniot experiments were conducted on an amorphous material of anorthite composition, in the pressure range 8–120 GPa, using both routine and new methods. Two Hugoniot measurements at about 120 GPa were made on lunar gabbroic anorthosite (*Apollo 15*, 418). Theoretical Hugoniots are constructed for both materials assuming they are disproportionate to their component oxides. These accurately predict the P–ρ behaviour of the lunar anorthosite Hugoniot at 120 GPa and the anorthite glass Hugoniot above 50 GPa, but overestimate the shock temperatures of anorthite glass. The mixed oxide model fails to predict the release paths of either material. We conclude that the mixed oxide model is a good description of the bulk properties of the high-pressure phases of anorthite, but does not represent the actual phases. A significant enrichment of calcic refractory material in the Earth's lower mantle is not precluded by the bulk properties of the anorthite high-pressure phases.

Key words: anorthite, anorthosite, compression, plagioclase, shock

Introduction

Anorthite is a mineral of considerable geophysical importance because it is among the first phases to condense in nebula models of the formation of the Solar System (Grossman & Larimer 1974). If the accretion process began before condensation was complete, the lower mantle would be expected to be enriched in refractories (Turekian & Clark 1969). Such an inhomogeneous model would predict that a high-pressure phase assemblage derived from anorthite is a major component of the lower mantle. Calculations based on cosmochemical abundances of Si, Mg, Al and Ca (Ross & Aller 1976) predict a mean mass fraction of 0.12 and 0.16 for an anorthite-composition phase in a predominantly enstatite- or forsterite-composition mantle, respectively.

Due to its geophysical importance, anorthite has been the subject of several shock wave

* Now at Sandia National Laboratories, Division 1131, Albuquerque, NM 87185, USA.

studies. McQueen, Marsh & Fritz (1967) conducted Hugoniot experiments on Tahawus anorthosite at pressures from 15 to 95 GPa. The samples used in that study were crystalline, and were 90 per cent plagioclase with 0.49 mole fraction anorthite, and initial densities ranging from 2.70 to 2.79 $Mg\,m^{-3}$. McQueen *et al.* (1967) inferred from their data that above about 33 GPa the Hugoniot enters a regime in which the shock states correspond to a high-pressure phase with a zero pressure density of between 3.46 and 3.53 $Mg\,m^{-3}$, and an initial isentropic bulk modulus of 88–112 GPa. This high-pressure phase gives a close match to the seismologically determined lower mantle density, but the inferred bulk modulus is considerably less than the lower mantle at comparable conditions.

Additional Hugoniot experiments of Ahrens, Peterson & Rosenburg (1969a) on plagioclase from 18 to 68 GPa also indicate a transition of this material to a high-pressure–high-density polymorph above 30 GPa. It was concluded in that study, and by Ahrens, Anderson & Ringwood (1969b) that the high-pressure polymorph corresponds to the hollandite structure.

Jeanloz & Ahrens (1980) carried out a series of Hugoniot experiments on lunar anorthosite 60025, which is about 18 per cent porous, and single-crystal Miyake-zima anorthite. Shock pressures attained ranged from 40 to 120 GPa. The porous data were used to determine the Gruneisen parameter, and a thermal equation of state was constructed for the high-pressure phase. The zero pressure density and initial isentropic bulk modulus were concluded to be 3.40 $Mg\,m^{-3}$ and 86.5 GPa, respectively, for the calculated Hugoniot which gave the best fit to the data inferred by the authors as belonging in the high-pressure regime, above 33 GPa. This is in close agreement with the lower values of McQueen *et al.* (1967). Jeanloz & Ahrens (1980) also concluded that, despite a close match in density to the lower mantle, the high-pressure phase or phase assemblage of anorthite is too compressible to constitute a major lower mantle component.

Boslough, Ahrens & Mitchell (1986) conducted shock-temperature experiments on anorthite glass in order to study its high pressure thermal behaviour further at pressures from 50 to 115 GPa and temperatures of 2500–5600 K. They found deviations in measured temperatures from what would be calculated assuming a simple single high-pressure phase model in this pressure range, and concluded that as many as three phase transitions might occur between 50 and 115 GPa, at about 55, 85 and 100 GPa. Shock-temperature experiments on anorthite glass were also carried out to about 40 GPa by Schmitt & Ahrens (1983). The high temperatures ($\approx$ 3000 K) measured in these experiments were assumed to be at the melting point of the high-pressure phase existing along shear bands in the shocked material.

The purpose of this paper is to present the first Hugoniot data on anorthite glass, and discuss it in context with the previous porous and single crystal Hugoniot data and shock-temperature data to generate a more complete self-consistent high-pressure equation of state. For comparison, new Hugoniot data are presented for a lunar recrystallized and brecciated gabbroic anorthosite (*Apollo 15,* 418). This rock was the subject of previous shock wave work by Ahrens, O'Keefe & Gibbons (1973) at pressures up to 28 GPa.

Experimental

Twenty-one experiments were carried out on anorthite glass using two different guns and four different experimental techniques. All four methods were based on measuring the shock velocity through the sample. First, the standard Hugoniot experiment, as described by Jeanloz & Ahrens (1977) was used (Fig. 1). Second, anorthite 'rider' mirrors were used in lieu of fused quartz mirrors on Hugoniot experiments which were primarily intended for other samples (Fig. 1). Third, shock transit times were measured from the oscillograms used

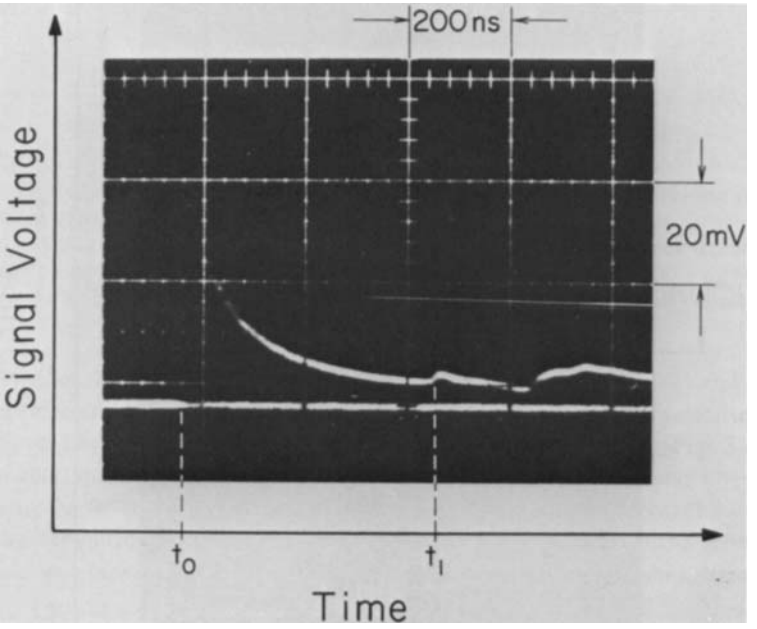

Figure 2. Oscilloscope record from 750 nm channel of optical pyrometer; shot LGG 132 (An6T) to 48 GPa. At time t_0, shock wave arrives at driver–sample interface. At t_1, shock reaches sample free surface.

[*facing page* 456]

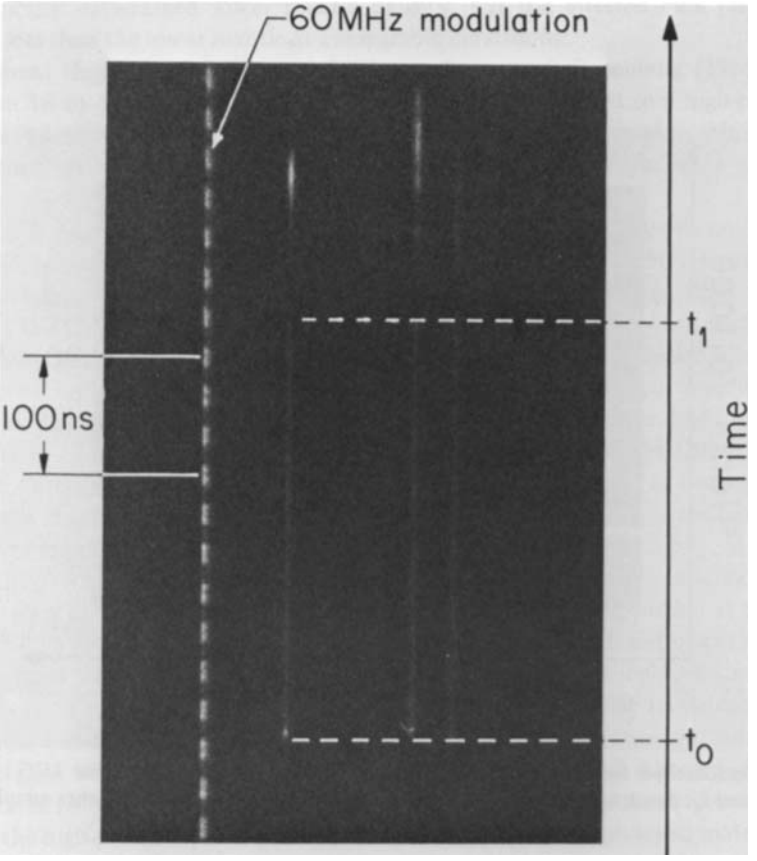

Figure 4. Streak camera record from shot LGG 136 to 92 GPa, illustrating use of optical fibres in conjunction with shock-temperature experiment to determine shock transit time. At time t_0, shock wave enters sample from opaque driver, and fibre collects thermally radiated light. At t_1, shock reaches sample–fibre interface and light intensity decreases. Time calibration is by a laser modulated at 60 MHz by a Pockels cell. Three of six fibre traces are shown.

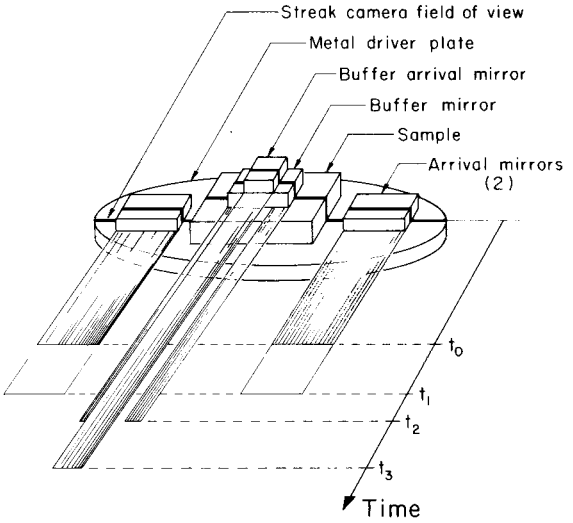

Figure 1. Configuration of standard Hugoniot experiments including schematic representation of streak. Times t_0, t_1, t_2 and t_3 correspond to shock wave arrival at: driver–arrival mirror interface, arrival mirror-free surface, sample–buffer mirror interface, buffer mirror–buffer arrival mirror interface, respectively. In ideal experiment (no shock tilt or bowing), transit times are: $(t_2 - t_0)$ for sample, $(t_1 - t_0)$ for arrival mirror, and $(t_3 - t_2)$ for buffer mirror. In the 'rider' experiment, arrival mirrors are made of anorthite glass.

primarily to determine the shock temperatures (Boslough *et al.* 1986) (Fig. 2) and finally, transit times were determined by obtaining streak camera records of light transmitted from the sample via optic fibres in several of the shock-temperature experiments (Figs 3 and 4). In some experiments, partially released states were also determined by attaching low-density buffer materials to the downstream surface of the samples. In two shots, fully released states were obtained by measuring the free surface velocity with an inclined mirror (Ahrens & Gregson 1964). Lower pressure experiments ($P < 40$ GPa) were performed on a 40 mm bore

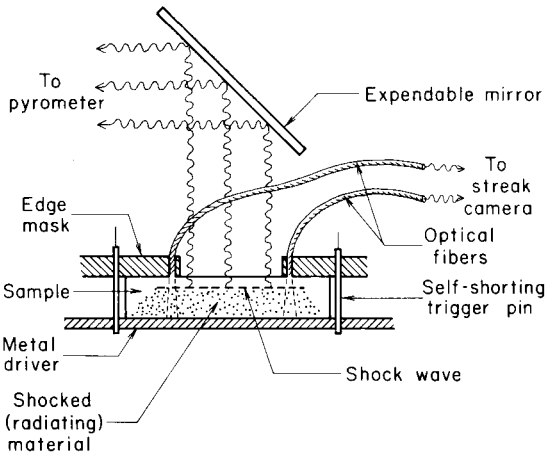

Figure 3. Configuration of shock-temperature experiments in which Hugoniot data are also obtained. In one method, the shock transit time is taken from the optical pyrometer oscilloscope records of the light radiated from the shocked sample. In the other method, light is collected by optical fibres and conducted to a streak camera.

propellant gun (Ahrens, Lower & Lagus 1971). High-pressure shots ($P > 40$ GPa) were carried out on a two-stage light-gas gun (Jeanloz & Ahrens 1977).

In all cases, the measured data were reduced to thermodynamic variables using the Rankine–Hugoniot relations:

$$P = \rho_0 U_s u_p, \tag{1}$$

$$\rho = \rho_0 \left(1 - \frac{u_p}{U_s}\right)^{-1}, \tag{2}$$

$$E - E_0 = \tfrac{1}{2} P (V_0 - V), \tag{3}$$

where P, ρ, E and V are the pressure, density, specific internal energy and specific volume $(1/\rho)$ of the shocked material, respectively. Those variables subscripted by zero are the initial (unshocked) values. U_s and u_p are the velocity of the shock wave and velocity of the material behind the shock wave (particle velocity), respectively. The method of impedance matching (Rice, McQueen & Walsh 1958) was used to obtain u_p from the measured impact velocity. The flyer/driver materials, and the sources of their respective Hugoniots used in the impedance match solution are: polycarbonate (Lexan), (Carter & Marsh 1977); aluminium 2024 and tungsten (McQueen *et al.* 1970), and copper and tantalum (Mitchell & Nellis 1981).

In the standard Hugoniot experiment (Fig. 1), a shock wave is generated by the impact of a light-gas gun or 40 mm gun-launched flyer plate with a stationary driver plate, on which are mounted the polished sample and two silvered quartz or polycarbonate arrival mirrors. After travelling through the driver plate, the shock enters the sample and mirrors. When the shock wave arrives at the driver–mirror interface, the lapped surface of the driver is driven into the specularly reflecting surface of the mirror, resulting in a rapid change in reflectivity which can be observed by monitoring the reflected light with a high speed Model 339B Beckman-Whitley continuous writing rotating mirror or TRW model 21A image converter streak camera. The shock wave continues through the sample to its other surface, where it impinges on a fused quartz or polycarbonate buffer mirror which changes its reflectivity in the same manner, providing a measure of the shock transit time through the sample. When the shock wave reflects from the buffer–sample interface, a rarefaction to a lower pressure state propagates back into the anorthite. Simultaneously a shock wave with the same pressure and particle velocity is driven into the buffer material. The arrival of this lower amplitude shock wave at the buffer material free surface is again detected by the loss of reflectivity of a buffer arrival mirror, which provides a measure of the shock transit time in the buffer. In some cases the buffer material was replaced by an inclined mirror whose angle of extinction allowed determination of the free surface velocity of the shocked sample. Solution of the Riemann integral (Rice *et al.* 1958; Lyzenga & Ahrens 1978) allowed determination of a partial (buffer) or full (inclined mirror) release state in the sample. The buffer materials and the sources of their respective Hugoniots used to determine partial release states are: polycarbonate (Carter & Marsh 1977); graphite foam, and polystyrene foam (Marsh 1980); fused silica (Jackson & Ahrens 1979); and NaCl (Kormer *et al.* 1965).

The 'rider' method is a modification of this experiment, in which the sample is not anorthite glass, but some other material for which the experiment is primarily intended (Fig. 1). The arrival mirrors, however, are fabricated out of anorthite glass. When the shock wave arrives at the driver–sample interface the silvered surfaces of the anorthite arrival mirrors lose their reflectivity in the usual way. The top, unsilvered surface of the mirror material continues to reflect at about 5 per cent this intensity, and does so until the shock reaches it. The light signal disappears within ≈ 2 ns of shock arrival, either as a result of shock tilt misaligning the free surface of the mirror in such a way that the light

reflected from the xenon light source misses the aperture of the streak camera, or due to disruption of the specular reflecting quality of the surface by an unknown process. This appears on the streak as a lighter image, from which the transit time through the anorthite glass mirror can be determined. The anorthite glass mirrors still serve the same functional purpose as the normal mirror in determining the Hugoniot of the primary material. The states determined for the anorthite glass by this method are not as precise as those determined by the standard method, because the rider mirrors are about half the thickness (≈ 1.1 mm) of the standard samples. This doubles the fractional error in the shock velocity measurement. A release state is not determined for anorthite glass with this method.

Hugoniot states were also determined in the shock-temperature experiments. The most straightforward method was simply to take the shock transit time from the oscilloscope shot records (Fig. 2), which display light intensity as a function of time (Boslough *et al.* 1986). This technique is less precise than the standard method for two reasons. First, the time resolution is limited by the rise times of the photodiodes, which are 1–7 ns. Second, the field of view of the photodiodes (2.3–6.4 mm) is much larger than the slit width of the streak camera (0.13 mm), so if the shock wave is not perfectly parallel to the sample surfaces (because of projectile tilt or slight misalignment) this will not be resolved. For some samples, the optical quality of the sample may preclude the use of this method in determining shock transit times (Boslough *et al.* 1986).

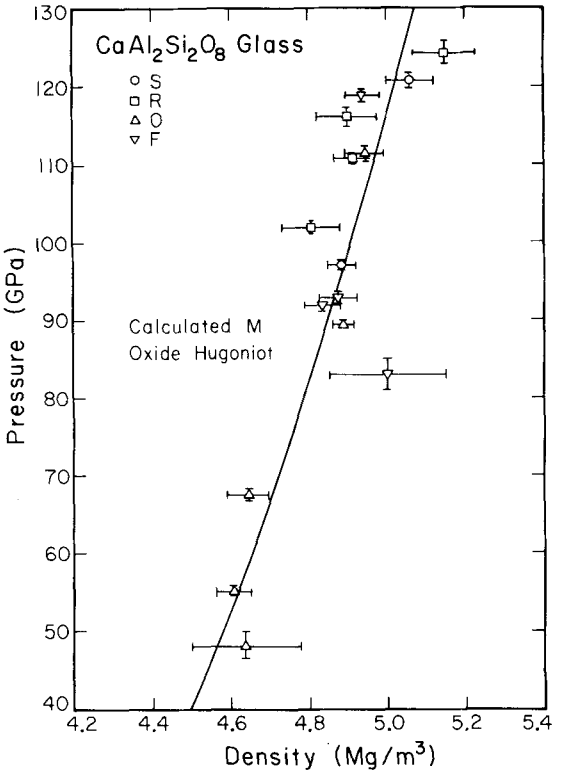

Figure 5. Anorthite glass Hugoniot data in the high-pressure regime from Table 1 plotted in the pressure–density plane, with theoretical mixed oxide Hugoniot based on parameters in Table 2. Data were obtained by four experimental methods: (S) Standard Hugoniot, (R) 'Rider' mirror, (O) Oscilloscope, (F) Optical fibre. These methods are described in the text.

Several of the shock-temperature targets were designed to allow the streak camera to be used in measuring the shock-transit time, with the intent on improving the precision over reading the oscillograms. Several 0.25 mm diameter, Poly-Optical Products Co., acrylic optical fibres with polished ends were attached to the free surface of the samples, and held in place by the edge mask (Fig. 3). When the shock wave enters the sample, thermal radiation is collected by the optic fibres and carried to the streak camera. When the shock reaches the sample–fibre interface, the light intensity changes due to the impedance mismatch as the shock is driven into the fibre itself. The transit time is obtained by measuring the length of the bright streak (Fig. 4). This technique is not degraded by shock wave tilt, as the field of view of the fibre is on the order of the fibre diameter itself. The time resolution is decreased somewhat, however, by the fact that the fibre diameter is 0.25 mm, as opposed to the slit width in the standard experiments of 0.13 mm. By using 0.13 mm diameter fibres, or mounting larger fibres behind the 0.13 mm wide slit, this method can achieve the same precision as the standard Hugoniot experiment. A shock temperature of about 3500 K in the sample, corresponding to a spectral radiance in the visible of about 10^{12} W Sr^{-1} m^{-3}, is required to produce enough light intensity to give a sufficient exposure of the film in the streak camera when 0.25 mm diameter fibres are used. If finer fibres are used, the required shock temperature will be higher. The required spectral radiance is approximately inversely proportional to the fibre diameter.

Results

The results of 21 Hugoniot measurements on anorthite glass are presented in Table 1 and shown in Figs 5–9. Previous data for Izu Island anorthite (Jeanloz & Ahrens 1980), porous

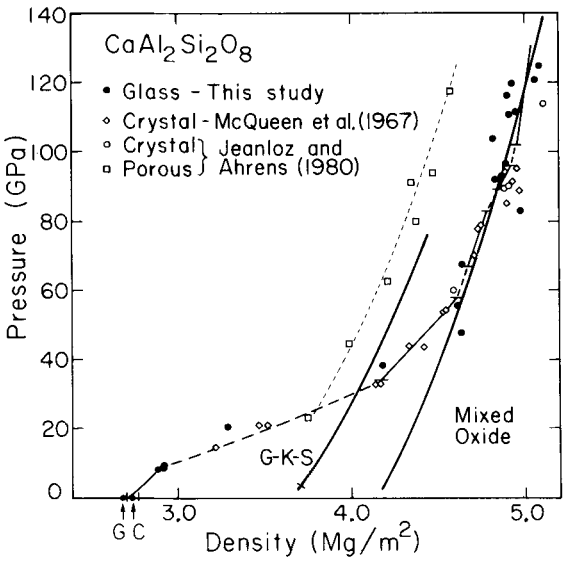

Figure 6. Anorthite glass Hugoniot data from this study, anorthite crystal and porous anorthosite data from Jeanloz & Ahrens (1980), and anorthite crystal data from McQueen *et al.* (1967). Solid and dashed curves give single phase and mixed phase regions, respectively, based on shock-temperature data (Boslough *et al.* 1986). Mixed oxide theoretical Hugoniot based on parameters in Table 2 gives good agreement with data above 55 GPa. Grossularite-kyanite-stishovite (G-K-S) theoretical Hugoniot does not agree with data anywhere. G and C refer to glass and crystalline initial densities, respectively.

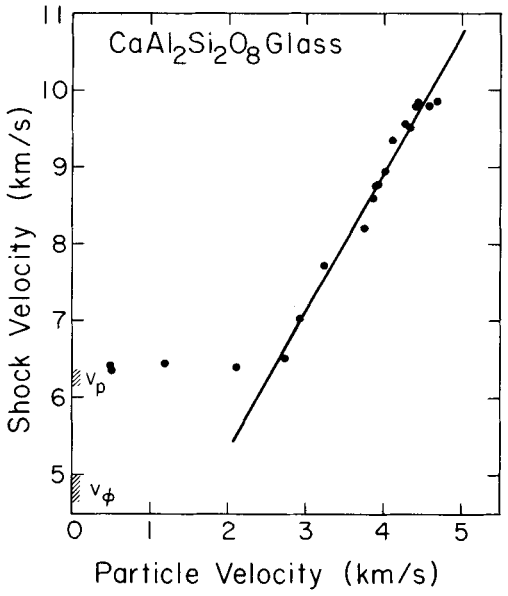

Figure 7. Hugoniot data for anorthite glass shown in the shock velocity–particle velocity plane. Best straight-line fit to high-pressure phase regime data is shown: $U_s = 1.82 + 1.77\,u_p$. v_ϕ and v_p are estimates of the bulk and compressional wave velocities.

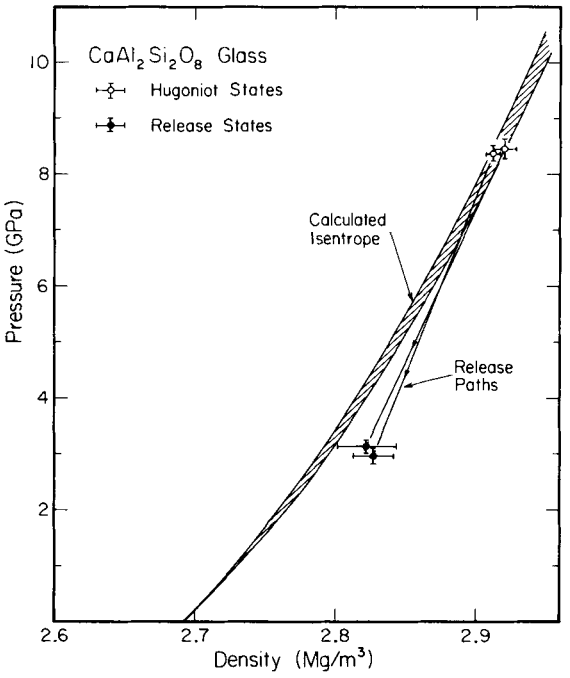

Figure 8. Anorthite glass Hugoniot data with measured release states. Curves are Birch–Murnaghan isentropes constrained by $K = 60.4$ GPa, $K' = 15$–16 and $K = 67.0$, $K' = 11.5$–12.5 to fit the shock wave data. Release paths suggest that irreversible compression can occur in anorthite glass at low pressures and are consistent with the calculated range of isentropes.

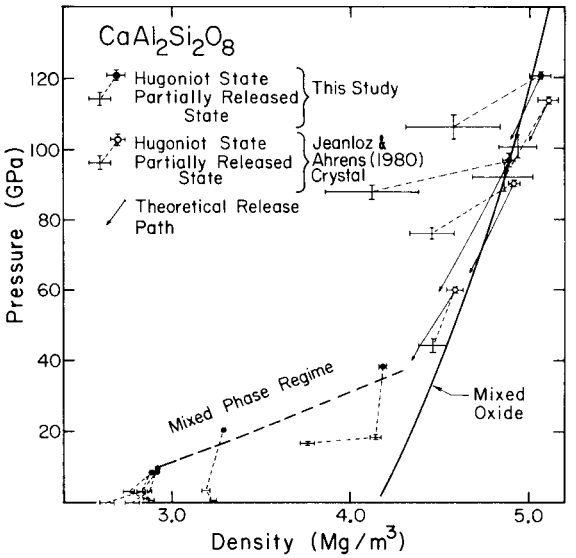

Figure 9. Anorthite glass and single crystal Hugoniot data, with measured release states. Theoretical mixed-oxide Hugoniot and corresponding theoretical release isentropes from experimental shock states are shown.

lunar anorthosite 60025 (Jeanloz & Ahrens 1978) and Tahawus anorthosite (McQueen *et al.* 1967) are also shown in Fig. 6 for comparison.

All but six data from the present study are in the high-pressure phase region, and are plotted in the $U_s - u_p$ plane in Fig. 7. The high-pressure phase data can be fitted by the linear relationship:

$$U_s = c_0 + su_p. \tag{4}$$

A least squares fit gives the values $c_0 = 1.82$ km s^{-1} and $s = 1.77$ with a coefficient of determination $r^2 = 0.98$. This equation can be used for impedance match solutions, and was used to determine the pressures in the shock-temperature experiments by Boslough *et al.* (1986).

The remaining data lie in the mixed phase region or in the low-pressure phase region and form an approximately horizontal trend in $U_s - u_p$ space (Fig. 7). Two samples have anomalously high shock velocities relative to the remainder and were excluded from the diagram. Poor shot records made these two experiments difficult to interpret and although they are included in Table 1, they will not be discussed further. A similar horizontal trend in $U_s - u_p$ space has been described by Wackerle (1962) for the mixed phase region of fused quartz.

None of the data show any indication of a two wave structure. This suggests that the data lie below the Hugoniot elastic limit (HEL) or sufficiently far above it that the elastic wave has been overridden. Particle velocities calculated from free surface velocities which were derived from inclined mirror experiments are compatible with particle velocities calculated by impedance matching. This is consistent with the observation of a single shock wave.

For crystalline feldspars HEL states are dependent upon driving shock pressure and vary upwards from 3.2 GPa for albite, 4.5 GPa for anorthosite (Ahrens & Gregson 1964) and 3.5 GPa for microcline (Ahrens & Liu 1973). For crystalline and fused quartz the lowest HEL states measured by Wackerle (1962) were 4.5 GPa. The states measured in this work for anorthite glass yield pressures on the order of 8 GPa. These pressures are considered to be

too high to represent states below the HEL and are suggested instead to be plastic deformational states well above the HEL.

Release data from the low-pressure phase regime and at the low-density end of the mixed phase region show generally steep release paths (Figs 8 and 9). At the high-density end of the mixed phase region the release path suggests reversion to a very low-density phase. This phenomena has been observed by Ahrens & Rosenberg (1968) for polycrystalline quartz and has been predicted theoretically by Zamyshlyaev, Ciovorukha & Shcherbatyuk (1982).

Low-pressure equation of state

The low-pressure equation of state can be usefully constrained using the two lowest pressure data. It was previously suggested that the HEL had been exceeded for these experiments. At shock states higher than the HEL for anorthite glass it is expected that all resistance to shear is lost and that it behaves as a fluid. This phenomenon has been observed in crystal and fused quartz (Wackerle 1962), perthitic feldspar (Grady, Murri & DeCarli 1975) and sapphire (Graham & Brooks 1971). It has been suggested (Grady *et al.* 1975) that the loss of shear strength is related to partial melting in shear bands behind the shock front. Shock-induced shear instabilities have also been reported for anorthite glass by Schmitt & Ahrens (1983) providing evidence that like other ceramic materials, anorthite glass loses all resistance to shear.

In the region above the HEL, with all resistance to shear lost, the Hugoniot should differ little from the hydrostat. In addition, at low pressures, thermal effects will be small and the Hugoniot will be well described by the principal isentrope.

No direct measurement of the bulk modulus of anorthite glass has been made but Young's modulus of an An_{70} glass measured by Birch & Bancroft (1942) is 89.9 GPa. A strong correlation between the product of Young's modulus (E) and ionic packing density (V_t), and the observed bulk modulus (K) for a set of 30 glasses of varying composition is observed by Makishima & MacKenzie (1975). This relation is given by $K = 1.2V_tE$ with V_t calculated from ionic radii and the component atoms normalized to glass density (Makishima & MacKenzie 1975). From this linear relation, the bulk modulus is estimated to be 60.4 GPa based on $E = 89.9$ GPa, the value measured by Birch & Bancroft (1942). Poisson's ratio for these values of K and E is 0.252.

Further constraints may be placed on the bulk modulus of anorthite glass using recent ultrasonic data from a variety of silicate glasses. Meister *et al.* (1980) measured the elastic moduli of a range of silicate glass compositions up to 0.8 GPa and noted a very good linear relation between bulk modulus and silica content. For anorthite glass this relation would predict a bulk modulus of 67 GPa, and a Poisson's ratio of 0.276, in reasonable agreement with the values calculated using the relation of Makishima & MacKenzie.

With these values of bulk modulus and an assumed Birth–Murnaghan equation of state K' may be determined from the Hugoniot data. As previously mentioned, it may be assumed at these pressures that the principal isentrope is coincident with the Hugoniot. For $K = 60.4$ GPa, $K' \approx 15$–16, and for $K = 67$ GPa, $K' \approx 11.5$–12.5 (Fig. 8). These values of K' suggest rapid stiffening of anorthite glass for moderate increases in pressure. For rock silicate glasses at pressures below 0.8 GPa, K' is less than 3 (Meister *et al.* 1980). Elastic parameters have been measured for fused quartz from atmospheric pressure to 13.3 GPa (Schroeder, Dunn & Bundy 1981). Above about 3 GPa, K' increases in a non-linear fashion and at 8 GPa, $K' \approx 7.5$. Boslough & Ahrens (1985) suggest that jadeite, in which Al is in octahedral coordination, is formed on the Hugoniot for anorthosite in the range 6–10 GPa.

Anorthite glass Hugoniot and release data.

Flyer material	Driver material	Projectile velocity (km s^{-1})	Initial density (Mg m^{-3})	Shock velocity (km s^{-1})	Particle velocity (km s^{-1})	Pressure (GPa)	Density (Mg m^{-3})	
Al-2024	Al-2024	0.95 ± 0.01	2.691 ± 0.002	6.85 ± 0.12	0.45 ± 0.01	8.32 ± 0.12	2.881	0.0
Partial release state 1 (Lexan buffer)				3.48 ± 0.05	0.73 ± 0.03	3.05 ± 0.18	2.76	0.0
Partial release state 2 (graphite foam buffer)				1.60 ± 0.02	0.62 ± 0.02	1.08 ± 0.04	2.85	0.0
Lexan	Al-2024	1.97 ± 0.01	2.697 ± 0.002	6.42 ± 0.05	0.484 ± 0.004	8.37 ± 0.06	2.912	0.0
Partial release state (Lexan buffer)				3.46 ± 0.03	0.72 ± 0.02	2.98 ± 0.11	2.827	0.0
Final release state (e) (inclined mirror)					1.02 ± 0.03	0.00	2.64	0.0
Al-2024	Al-2024	1.00 ± 0.02	2.693 ± 0.002	6.36 ± 0.04	0.49 ± 0.01	8.46 ± 0.18	2.920	0.0
Partial release state (Lexan buffer)				3.50 ± 0.03	0.745 ± 0.019	3.12 ± 0.11	2.822	0.0
Al-2024	Al-2024	1.105 ± 0.010	2.692 ± 0.002	6.745 ± 0.005	0.534 ± 0.006	9.69 ± 0.10	2.923	0.0
Partial release state 1 (Lexan buffer)				3.47 ± 0.04	0.726 ± 0.025	3.01 ± 0.14	2.876	0.0
Final release state (e) (inclined mirror)					0.87 ± 0.02	0.00	2.79	0.0
Partial release state 2 (polystyrene foam buffer)				1.07 ± 0.05	0.74 ± 0.04	0.045 ± 0.005	2.886	0.0
Al-2024	Al-2024	2.266 ± 0.003	2.693 ± 0.002	6.46 ± 0.06	1.179 ± 0.005	20.52 ± 0.11	3.295	0.0
Partial release state 1 (Lexan buffer)				3.53 ± 0.04	0.764 ± 0.025	3.227 ± 0.144	3.19	0.0
Partial release state 2 (polystyrene foam buffer)				1.94 ± 0.02	1.52 ± 0.02	0.165 ± 0.004	3.235	0.0
W	Cu	2.455 ± 0.005	2.693 ± 0.002	6.40 ± 0.04	2.283 ± 0.005	39.35 ± 0.20	4.186	0.0
Partial release state 1 (Lexan buffer)				6.24 ± 0.08	2.49 ± 0.05	18.59 ± 0.62	4.15	0.0
Partial release state 2 (graphite foam buffer)				4.89 ± 0.05	3.15 ± 0.04	16.67 ± 0.37	3.67	± 0.0

(An 6T)	Cu	Cu	3.72 ± 0.10	2.6908 ± 0.0010	6.508 ± 0.092	2.731 ± 0.078	47.8 ± 1.5	4.637 ± 0.1
(An 5T)	Cu	Cu	4.038 ± 0.002	2.6909 ± 0.0013	7.027 ± 0.081	2.929 ± 0.008	55.4 ± 0.5	4.615 ± 0.0
380 (An 3T)	Cu	Cu	4.536 ± 0.006	2.6900 ± 0.0010	7.717 ± 0.103	3.248 ± 0.011	67.4 ± 0.7	4.645 ± 0.0
(An 9T)	Cu	Cu	5.255 ± 0.003	2.6953 ± 0.0012	8.187 ± 0.240	3.755 ± 0.025	82.9 ± 1.9	4.978 ± 0.1
580 (An 2T)	Cu	Cu	5.455 ± 0.010	2.6899 ± 0.0011	8.598 ± 0.050	3.868 ± 0.009	89.5 ± 0.4	4.890 ± 0.0
	Cu	Cu	5.506 ± 0.003	2.6923 ± 0.0011	8.769 ± 0.085	3.889 ± 0.009	91.8 ± 0.7	4.838 ± 0.0
(An 7T)	Cu	Cu	5.563 ± 0.006	2.6927 ± 0.0011	8.782 ± 0.093	3.931 ± 0.011	93.0 ± 0.8	4.875 ± 0.0
	Cu	Cu	5.709 ± 0.003	2.6894 ± 0.0018	8.956 ± 0.068	4.027 ± 0.008	97.0 ± 0.6	4.856 ± 0.0
	Partial release state (fused quartz buffer)				8.512 ± 0.095	3.930 ± 0.051	73.7 ± 1.8	4.877 ± 0.0
	Cu	Cu	5.892 ± 0.005	2.6912 ± 0.0018	9.352 ± 0.152	4.126 ± 0.016	103.8 ± 1.3	4.816 ± 0.0
	Cu	Cu	6.166 ± 0.004	2.6912 ± 0.0018	9.535 ± 0.090	4.317 ± 0.010	110.8 ± 0.8	4.917 ± 0.0
380 (An 1T)	Ta	Ta	5.678 ± 0.010	2.6893 ± 0.0011	9.525 ± 0.100	4.348 ± 0.012	111.4 ± 1.0	4.948 ± 0.0
	Cu	Cu	6.328 ± 0.004	2.6912 ± 0.0018	9.785 ± 0.160	4.415 ± 0.017	116.2 ± 1.5	4.900 ± 0.0
(An 10T)	Ta	Cu	5.562 ± 0.003	2.6944 ± 0.0012	9.839 ± 0.089	4.470 ± 0.010	118.5 ± 0.8	4.938 ± 0.0
	Cu	Cu	6.547 ± 0.004	2.6924 ± 0.0020	9.784 ± 0.106	4.582 ± 0.012	120.7 ± 1.0	5.064 ± 0.0
	Partial release state (fused quartz buffer)				9.328 ± 0.153	4.371 ± 0.083	89.9 ± 3.2	5.027 ± 0.0
	Ta	Ta	6.140 ± 0.005	2.6903 ± 0.0014	9.843 ± 0.136	4.698 ± 0.013	124.4 ± 1.4	5.146 ± 0.0

rd equation of state experiment.
'riders' – (density from mean of other shots).
t time from shock-temperature oscilloscope records.
t time from optic fibres to streak camera.
rface velocity listed as particle velocity.

Development of some octahedral aluminium on the anorthite glass Hugoniot could lead to substantial stiffening and the observed strong dependence of bulk modulus on pressure.

High-pressure equation of state

The shock temperature data of Boslough *et al.* (1986) suggest the possibility for three phase transitions above 50 GPa on the principal Hugoniot of anorthite glass. The temperature data were used to estimate where the inferred phase boundaries cross the Hugoniot, and this information was transformed to the $P-\rho$ plane in Fig. 6, where single- and mixed-phase regions are delineated along the Hugoniot. These inferred phase transitions are not evident from the $P-\rho$ Hugoniot data, except perhaps between 80 and 90 GPa, where within the scatter in the data, there appears to be a sudden increase in density with pressure.

The inferred highest pressure phases are only stable on the Hugoniot in a density range of about 0.1 $Mg\,m^{-3}$, or about 5 per cent of their density, which is the same order as the scatter in the data. This makes it impossible to carry out a meaningful finite strain fit to the data in the individual regions of stability, in which several of the parameters: zero pressure density, K_0, and K'_0 are constrained independently. One alternative is to fix one parameter and determine what values the others must have in order to fit the data. This method does not, however, lead to a unique solution.

Another strategy which can be used is to choose a candidate phase or assemblage, *a priori* and determine its high-pressure properties. It can then be compared to the data directly and accepted or rejected as a candidate on this basis. This is similar to the approach of Davies & Gaffney (1973). We used a mixed oxide model as the candidate high-pressure assemblage, with CaO in the B2 phase (CsCl structure), Al_2O_3 as corundum and SiO_2 as stishovite.

The isentrope for the composite mixed oxide assemblage was constructed from the isentropes of the individual oxides. Molar volumes as a function of pressure were determined for each of the oxides using the Birch–Murnaghan equation and published values of K_{os} and K'_{os} (Table 2). The values for B2 CaO were taken from Boslough, Ahrens & Mitchell (1984), corundum from Anderson (1973) and stishovite from Lyzenga, Ahrens & Mitchell (1983). The molar volumes at a given pressure were added to give the molar volume of the composite, from which the pressure–density isentrope was obtained to 100 GPa. K_{os} = 227 GPa and

Table 2. Mixed oxide parameters – anorthite glass.

	CaO (B2)	Al_2O_3 (corundum)	SiO_2 (stishovite)	$CaAl_2Si_2O_8$ (composite)
ρ_0 (g)	4.00	3.986	4.29	4.07
K_{os} (GPa)	121	250	306	222
K'_{os}	5.2	4.0	5.4	5.1
γ	1.80	1.32	1.38	1.44
n	1.0	1.0	3.2	1.7
E_{tr} ($kJ\,g^{-1}$)	2.1	–	0.82[a]	0.87[b]
m_i	0.202	0.366	0.432	1.00
v_i	0.216	0.374	0.410	1.00
Reference	(c)	(d)	(e)	

[a] Robie, Hemingway & Fisher (1979).
[b] Includes 0.09 kJ^{-1} energy of formation of anorthite glass oxides at standard conditions (Robie *et al.* 1979).
[c] Boslough *et al.* (1984).
[d] Anderson (1973).
[e] Lyzenga *et al.* (1983).

$K'_{os} = 5.1$ were determined for the composite by carrying out a Birch–Murnaghan least squares fit to the calculated isentrope. The zero pressure bulk modulus calculated in this way is comparable to the Voigt–Reuss–Hill value of 228 GPa, and lies within the Voigt and Reuss bounds of 212 and 244 GPa, respectively (Watt, Davies & O'Connell 1976).

The Grüneisen parameter (γ) for the composite was calculated by taking the mean of the components, weighted according to mass fraction. Although this is not strictly correct (Duvall & Taylor 1971, it is a reasonable approximation. The energy of transformation between anorthite glass and the metastable high-pressure assemblage at standard conditions E_{tr} was obtained from the difference between the sum of E_{tr} for the oxides, and E_{tr} for anorthite glass, with the stable oxides as the reference state.

A Hugoniot was calculated for the composite mixed oxides, with anorthite glass as the initial state. This theoretical Hugoniot is in agreement with shock wave data above 60 GPa (Figs 5 and 6), but the temperatures predicted by this model are as much as 1500 K higher than those measured (Boslough *et al.* 1986). In order to fit data in both the P–ρ and P–T planes, a somewhat larger transition energy is required.

For comparison, a Hugoniot was calculated in the same manner for an assemblage consisting of $Ca_3Al_2SiO_3O_{12}$ (grossularite), Al_2SiO_5 (kyanite), and SiO_2 (stishovite), which is the stable phase at 15 GPa according to Liu (1978). This assemblage has a zero pressure density of 3.61 Mg m^{-3} and a Voigt–Reuss–Hill bulk modulus of 170 GPa. A range of Hugoniots was calculated for this phase, with $3.0 \geqslant \gamma_0 \geqslant 2.0$ and $\gamma = \gamma_0(\rho_0/\rho)$. This calculated Hugoniot is steeper than the observed Hugoniot (Fig. 6) and crosses it at about 30 GPa.

Discussion

It was concluded by Boslough *et al.* (1986) that, due to the complicated behaviour observed in the anorthite Hugoniot in the P–T plane, a simple equation of state is probably insufficient to describe this material at high pressure. It is evident, however, that the mixed oxide assemblage is a good model for the behaviour in the P–ρ plane above 60 GPa whereas the grossularite-kyanite-stishovite assemblage is not a good description in any pressure regime. The Jeanloz & Ahrens (1980) equation of state adequately describes the data in both P–ρ and P–T planes from 33 to 60 GPa.

Comparison of the calculated mixed oxide Hugoniot to data in the P–T plane (Boslough *et al.* 1986) gives evidence that the high-pressure phase is not mixed oxides, but a phase with similar bulk properties and a greater energy of transformation. Above 55 GPa, $CaAl_2Si_2O_8$ probably undergoes further phase transitions, and each higher pressure phase has a larger total energy of transformation. These higher phase transitions are sufficient to lower the shock temperature, but are not significant in the P–ρ plane, implying only a small volume change is associated with each phase transition. The porous Hugoniot was determined experimentally by Jeanloz & Ahrens (1978, 1980), and does not agree with that calculated using the mixed oxide model, which predicts higher densities at a given shock pressure. In light of the complexity of the high-pressure properties of $CaAl_2Si_2O_8$, a reasonable explanation for this is that the porous data do not represent the same phase as the non-porous data, but rather a lower pressure or higher temperature, less dense phase.

It must be remembered that, even though the mixed oxide Hugoniot fits the data well globally, the true Hugoniot may go through several phase transitions, with each phase stable only along a short segment of the Hugoniot, where material properties such as the bulk modulus and Gruneisen parameter may differ greatly from those of the mixed oxides. Perhaps a better determination of the local compressibilities would be from partial release data. Fig. 9 shows that, in fact, the release paths do vary greatly with pressure along the glass

and single crystal Hugoniots. Of the four high-pressure phase regimes inferred from the shock temperature data by Boslough *et al.* (1986), three are sampled by the five highest pressure Hugoniot-release experiments in this study and that of Jeanloz & Ahrens (1980). The release paths from the two highest pressure anorthite glass Hugoniot-release experiments are very shallow. This may indicate partial vaporization upon release, consistent with entropy gain calculations of Boslough & Ahrens (1983) which predict an incipient shock vaporization pressure of 92 GPa. One experimental data point for crystalline anorthite at about 60 GPa, lies just above the lowest inferred high-pressure phase regime, and its release path is slightly steeper than predicted. Highly variable release paths were also observed in porous anorthite (Jeanloz & Ahrens 1978, 1980) and in some cases the release paths were steeper than the Hugoniot inferred in that study. Unfortunately, partial release data are generally of lower quality than Hugoniot data.

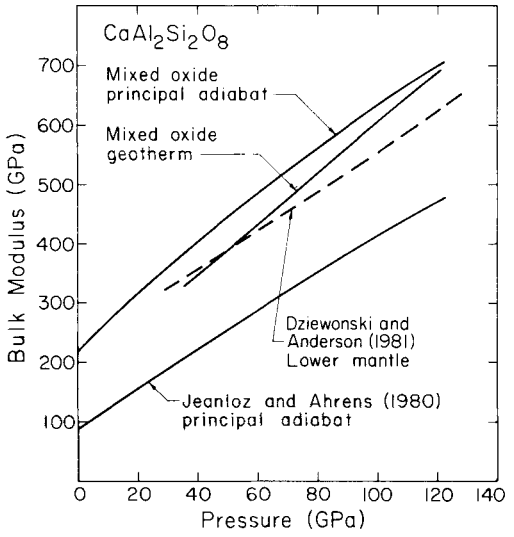

Figure 10. Adiabatic bulk modulus of the mixed oxide model as a function of pressure on principal adiabat and geotherm (Stacey 1977). Also shown is the bulk modulus of mantle as determined from seismological data (Dziewonski & Anderson 1981), and anorthite adiabat of Jeanloz & Ahrens (1980).

It is interesting to compare the mixed oxide adiabat to that of the lower mantle, determined seismologically (Dziewonski, Hales & Lapwood 1975; Anderson & Hart 1976; Dziewonski & Anderson 1981). Comparison is made with the most recent of these seismological models in Figs 10–12. In order to make a meaningful comparison, it is necessary to correct the theoretical mixed oxide adiabat to temperatures existing in the mantle. The geotherm of Stacey (1977) was used. Whereas Jeanloz & Ahrens (1980) found the bulk modulus much too low for anorthite to be a significant component of the lower mantle, the mixed oxide model gives a bulk modulus that is somewhat high, but closer to the seismologically determined lower mantle value. Thus, the high-pressure phases of anorthite should not be precluded as major constituents of the lower mantle, especially in light of the fact that there are probably unresolved phases on the Hugoniot which have bulk moduli which might deviate significantly in either direction from that of the mixed oxide composite.

Lunar anorthosite

In addition to anorthite glass, two experiments were conducted on lunar gabbroic anorthosite (*Apollo 15*, 418). These experiments were carried out with the standard method (Fig. 1),

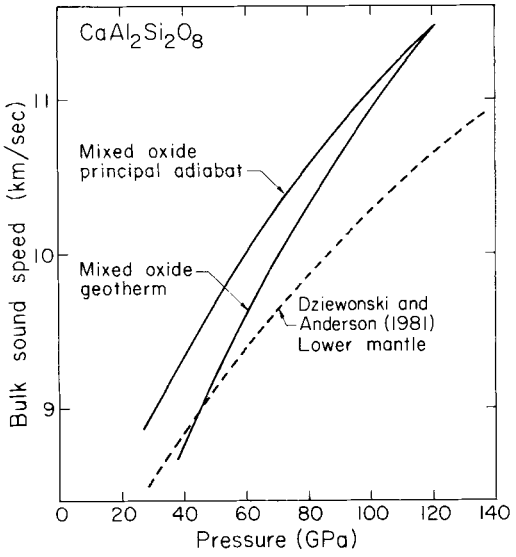

Figure 11. Bulk sound speed of the mixed oxide model as a function of pressure on principal adiabat and geotherm (Stacey 1977), compared to seismologically determined curve for the Earth's mantle (Dziewonski & Anderson 1981).

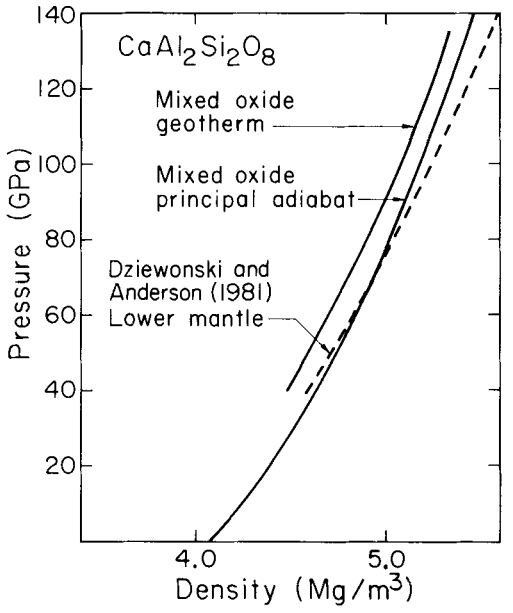

Figure 12. Pressure as a function of density for the mixed oxide principal adiabat and geotherm (Stacey 1977) compared to seismologically determined densities (Dziewonski & Anderson 1981).

and partial release states were determined in both cases. The results are presented in Table 3 and Fig. 13. This rock was modelled as 0.74 volume fraction anorthite (an_{93}) and 0.26 volume fraction enstatite (en_{64}) by Ahrens *et al.* (1973), taken from a microprobe analysis. In order to construct a theoretical mixed oxide Hugoniot for this rock, as was done for

Table 3. *Apollo 15*, 418 Hugoniot and release data.

Shot	Flyer material	Driver material	Projectile velocity ($km\ s^{-1}$)	Initial density ($Mg\ m^{-3}$)	Shock velocity ($km\ s^{-1}$)	Particle velocity ($km\ s^{-1}$)	Pressure (GPa)	Density ($Mg\ m^{-3}$)
LGG 119	Ta	Ta	5.823 ± 0.005	2.8414 ± 0.0014	9.811 ± 0.060	4.397 ± 0.007	122.6 ± 0.6	5.149 ± 0.031
	Partial release state (NaCl buffer)				9.838 ± 0.018	4.752 ± 0.014	101.2 ± 0.5	4.998 ± 0.033
LGG 118	Ta	Ta	5.830 ± 0.005	2.8914 ± 0.0022	9.907 ± 0.035	4.380 ± 0.005	125.5 ± 0.4	5.183 ± 0.018
	Partial release state (graphite foam buffer)				9.170 ± 0.031	6.446 ± 0.024	63.9 ± 0.5	3.813 ± 0.032

anorthite glass, we assumed the plagioclase fraction to be pure anorthite, due to our ignorance of the high-pressure behaviour of Na_2O, and the observation that anorthite and albite have similar Hugoniots (McQueen *et al.* 1967). The resulting mass fractions in the simplified model are 0.70 for anorthite ($CaAl_2Si_2O_8$), 0.19 for enstatite ($MgSiO_3$), and 0.11 for ferrosilite ($FeSiO_3$). These are broken down into their five component oxides (Table 4), and a high-pressure adiabat and Hugoniot were constructed in the same manner as for anorthite glass. The theoretical Hugoniot constructed in this way is seen in Fig. 13 to give excellent agreement to the Hugoniot data, and to the initial slope of the measured release path. As in the case of pure anorthite, it is not likely that the lunar rock disproportionates into its component oxides at these pressures, but the mixed oxide model gives a good description of the bulk properties of whatever phases exist there. The second release datum indicates a large density decrease upon unloading, consistent with shock-vaporization of material. Entropy-gain calculations of Ahrens & O'Keefe (1977) indicate that incipient vaporization may occur at shock pressures above 102 GPa for gabbroic anorthosite.

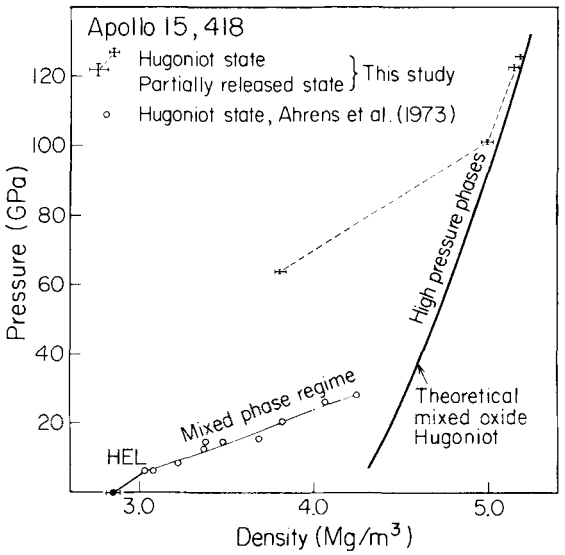

Figure 13. Lunar gabbroic anorthosite Hugoniot and release data. Mixed oxide theoretical Hugoniot based on parameters in Table 4 gives good agreement with data. One partial release state was determined for each shock state, but because shock states are so close, the two separate partial release states are connected in the illustration to outline an approximate release path.

Table 4. Mixed oxide parameters – lunar gabbroic anorthosite.

	CaO (B2)	Al_2O_3 (corundum)	SiO_2 (stishovite)	MgO (B1)	FeO (B2)	Composite
ρ_0 (g)	4.00	3.986	4.29	3.56	6.05	4.14
K_{os} (GPa)	121	250	306	170	195	219
K'_{os}	5.2	4.0	5.4	4.0	3.4	5.1
γ	1.80	1.32	1.38	1.3	1.8	1.44
n	1.0	1.0	3.2	1.0	1.25	1.8
E_{tr} (kJ g^{-1})	2.1	–	0.8[a]	–	0.4	1.01[b]
m_i	0.141	0.257	0.466	0.076	0.060	1.00
ν_i	0.154	0.267	0.450	0.089	0.041	1.00
References	(c)	(d)	(e)	(f)	(g)	

[a] Robie *et al.* (1979).
[b] Includes 0.35 kJ g^{-1} energy of formation of anorthite and 0.35 kJ g^{-1} energy of formation of enstatite from oxides (Robie *et al.* 1979).
[c] Boslough *et al.* (1984).
[d] Anderson (1973).
[e] Lyzenga *et al.* (1983).
[f] Vassiliou & Ahrens (1981).
[g] Jeanloz & Ahrens (1980).

Conclusions

The experimental Hugoniots of anorthite glass above 60 GPa and lunar gabbroic anorthosite at 120 GPa are well described by the Hugoniots calculated for their composite oxides, based on the individual properties of the oxides. The actual phases which are stable along the Hugoniot of anorthite, however, have larger energies of transformation. The zero pressure density of the mixed-oxide high-pressure phase assemblage model is 4.07 Mg m^{-3}, and the zero-pressure bulk modulus is 228 GPa. These values are comparable to those for the lower mantle, indicating that $CaAl_2Si_2O_8$, or its high-pressure reaction products, cannot be precluded as major components of the lower mantle on the basis of its equation of state. Such a refractory component could therefore be present in the lower mantle with a mass fraction in the range 0.12–0.16 as predicted by cosmochemical abundance considerations (Ross & Aller 1976), or in greater concentrations as expected by inhomogeneous accretion models (Turekian & Clark 1969).

Acknowledgments

We wish to thank E. Bus, E. Gelle, W. Ginn, M. Long and C. Manning for their excellent technical help, and J. Bass for informative discussions. Support was provided by NASA NGL 5-002-105 and NSG 0019. Several data are derived from shock-temperature measurements carried out at Lawrence Livermore National Laboratory. We are grateful to A. C. Mitchell and W. J. Nellis for the use of their light gas gun facility. Contribution 3997, Division of Geological and Planetary Sciences, California Institute of Technology.

References

Ahrens, T. J., Anderson, D. L. & Ringwood, A. E., 1969b. Equations of state and crystal structures of high-pressure phases of shocked silicates and oxides, *Rev. Geophys.*, 7, 667–707.

Ahrens, T. J. & Gregson, V. G. (Jr), 1964. Shock compression of crustal rocks: data for quartz, calcite and plagioclase rocks, *J. geophys. Res.*, 69, 4839–4874.

Ahrens, T. J. & Liu, H.-P., 1973. A shock-induced phase change in orthoclase, *J. geophys. Res.*, 78, 1274–1278.

Ahrens, T. J., Lower, J. H. & Lagus, P. L., 1971. Equation of state of forsterite, *J. geophys. Res.*, 76, 518–528.

Ahrens, T. J. & O'Keefe, J. D., 1977. Equations of state and impact-induced shock-wave attenuation on the moon, in *Impact and Explosion Cratering*, pp. 639–656, eds Roddy, D. J., Pepin, R. O. & Merrill, R. B., Pergamon Press, New York.

Ahrens, T. J., O'Keefe, J. D. & Gibbons, R. V., 1973. Shock compression of a recrystallized anorthositic rock from *Apollo 15, Proc. 4th Lunar Sci. Conf.*, pp. 63–64.

Ahrens, T. J., Peterson, C. F. & Rosenberg, J. T., 1969a. Shock compression of feldspars, *J. geophys. Res.*, 74, 2727–2746.

Ahrens, T. J. & Rosenberg, J. T., 1968. Shock metamorphism: experiments on quartz and plagioclase, in *Shock Metamorphism of Natural Materials*, pp. 59–81, eds French, B. M. & Short, W. M., Mono Press, Baltimore.

Anderson, D. L. & Hart, R. S., 1976. An earth model based on free oscillations and body waves, *J. geophys. Res.*, 81, 1461–1475.

Anderson, O. L., 1973. A scaling law for K'_0 for silicates with constant mean atomic mass, *Earth planet. Sci. Lett.*, 20, 73–76.

Birch, F. & Bancroft, D., 1942. The elasticity of glass at high temperatures, and the vitreous basaltic substratum, *Am. J. Sci.*, 240. 457–490.

Boslough, M. B. & Ahrens, T. J., 1983. Shock-melting and vaporization of anorthosite and implications for an impact-origin of the moon, *Lunar and Planetary Science XIV*.

Boslough, M. B. & Ahrens, T. J., 1985. Shock wave properties of anorthosite and gabbro, *J. geophys. Res.*, 90, 7814–7820.

Boslough, M. B., Ahrens, T. J. & Mitchell, A. C., 1984. Shock temperatures in CaO, *J. geophys. Res.*, 89, 7845–7851.

Boslough, M. B., Ahrens, T. J. & Mitchell, A. C., 1986. Shock temperatures in anorthite glass, *Geophys. J. R. astr. Soc.*, 84, 475–489

Carter, W. J. & Marsh, S. P., 1977. Hugoniot equations of state of polymers, *unpublished report LA-UR-77-2062*, Los Alamos Scientific Laboratory.

Davies, G. F. & Gaffney, E. S., 1973. Identification of high-pressure phases of rocks and minerals from Hugoniot data, *Geophys. J. R. astr. Soc.*, 33, 165–183.

Duvall, G. E. & Taylor, S. M. (Jr), 1971. Shock parameters of a two component mixture, *J. Compos. Mater.*, 5, 130–139.

Dziewonski, A. D. & Anderson, D. L., 1981. Preliminary reference earth model, *Phys. Earth planet. Int.*, 25, 297–356.

Dziewonski, A. M., Hales, A. L. & Lapwood, E. R., 1975. Parametrically simple earth models consistent with geophysical data, *Phys. Earth planet. Int.*, 10, 12–48.

Grady, D. E., Murri, W. J. & DeCarli, P. S., 1975. Hugoniot sound velocities and phase transformations in two silicates, *J. geophys. Res.*, 80, 4857–4861.

Graham, R. A. & Brooks, W. P., 1971. Shock-wave compression of sapphire from 15 to 4000 kBar: the effects of large anisotropic compressions, *J. Phys. Chem. Solids*, 32, 2311–2330.

Grossman, L. & Larimer, J. W., 1974. Early chemical history of the solar system, *Rev. Geophys. Space Phys.*, 12, 71–101.

Jackson, I. & Ahrens, T. J., 1979. Shock-wave compression of single-crystal forsterite, *J. geophys. Res.*, 84, 3039–3048.

Jeanloz, R. & Ahrens, T. J., 1977. Pyroxenes and olivines: structural implications of shock-wave data for high pressure phases, in *High-Pressure Research*, pp. 439–461, eds Manghnani, M. & Akimoto, S., Academic Press, New York.

Jeanloz, R. & Ahrens, T. J., 1978. The equation of state of a lunar anorthosite: 60025, *Proc. 9th Lunar Planet. Sci. Conf.*, pp. 2789–2803.

Jeanloz, R. & Ahrens, T. J., 1980. Anorthite: thermal equation of state to high pressures, *Geophys. J. R. astr. Soc.*, 62, 529–549.

Kormer, S. B., Sinitsyn, M. V., Funtikov, A. I., Urlin, V. D. & Blinov, A. V., 1965. Investigation of the compressibility of five ionic compounds at pressures up to 5 Mbar, *Soviet Phys. JETP*, 20, 811–819.

Liu, L.-G., 1978. A new high-pressure phase of $Ca_2Al_2SiO_7$ and implications for the earth's interior, *Earth planet. Sci. Lett.*, 40, 401–406.

Lyzenga, G. & Ahrens, T. J., 1978. The relations between the shock-induced free-surface velocity and post-shock density of solids, *J. appl. Phys.*, **49**, 201–204.

Lyzenga, G. A., Ahrens, T. J. & Mitchell, A. C., 1983. Shock temperatures of SiO_2 and their geophysical implications, *J. geophys. Res.*, **88**, 2431–2444.

Makishima, A. & MacKenzie, J. D., 1975. Calculation of bulk modulus, shear modulus and Poisson's ratio of glass, *J. Non. Cryst. Solids*, **17**, 147–157.

Marsh, S. P. (ed.), 1980. *LASL Shock Hugoniot Data*, University of California Press, Berkeley.

McQueen, R. G., Marsh, S. P. & Fritz, J. N., 1967. Hugoniot equations of state of twelve rocks, *J. geophys. Res.*, **72**, 4999–5036.

McQueen, R. G., Marsh, S. P., Taylor, J. W., Fritz, J. N. & Carter, W. J., 1970. The equation of state of solids from shock wave studies, in *High Velocity Impact Phenomena*, pp. 294–419, ed. Kinslow, R., Academic Press, New York.

Meister, R., Robertson, E. C., Werre, R. W. & Raspet, R., 1980. Elastic moduli of rock glasses under pressure to 8 kilobars and geophysical implications, *J. geophys. Res.*, **85**, 6461–6470.

Mitchell, A. C. & Nellis, W. J., 1981. Shock compression of aluminum, copper, and tantalum, *J. appl. Phys.*, **52**, 3363–3374.

Rice, M. H., McQueen, R. G. & Walsh, J. M., 1958. Compressibility of solids by strong shock waves, *Solid St. Phys.*, **6**, 1–63.

Robie, R. A., Hemingway, B. S. & Fisher, J. R., 1979. *Thermodynamic properties of minerals and related substances at 298.15 K and 1 Bar (10^5 Pascals) pressure and at higher temperatures*, Government Printing Office, Washington, DC.

Ross, J. E. & Aller, L. H., 1976. The chemical composition of the sun, *Science*, **191**, 1223–1229.

Schmitt, D. R. & Ahrens, T. J., 1983. Temperatures of shock-induced shear instabilities and their relationship to fusion curves, *Geophys. Res. Lett.*, **10**, 1077–1080.

Schroeder, J., Dunn, K.-J. & Bundy, F. P., 1981. *Brillouin scattering from amorphous SiO_2 under hydrostatic pressure up to 133 kBar*, General Electric Corporate Research and Development Report 81CRD216.

Stacey, F. D., 1977. A thermal model of the earth, *Phys. Earth planet. Int.*, **15**, 341–348.

Turekian, K. K. & Clark, S. P. (Jr), 1969. Inhomogeneous accretion model of the earth from the primitive solar nebula, *Earth planet. Sci. Lett.*, **6**, 346–348.

Vassiliou, M. S. & Ahrens, T. J., 1981. Hugoniot equation of state of periclase to 200 GPa, *Geophys. Res. Lett.*, **8**, 729–732.

Wackerle, J., 1962. Shock wave compression of quartz, *J. appl. Phys.*, **33**, 922–937.

Watt, J. P., Davies, G. F. & O'Connell, R. J., 1976. The elastic properties of composite materials, *Rev. Geophys. Space Phys.*, **14**, 541–563.

Zamyshlyaev, B. V., Ciovorukha, E. A. & Shcherbatyuk, V. A., 1982. Polymorphic phase transformations in the presence of dynamical interactions, *Soviet Phys. Dokl.*, **27**, 324–326.